

Numerical Study on Breaking Wave Interaction with Vertical Wall Attached with Recurved Parapet

Songtao Chen*, Weiwen Zhao*† and Decheng Wan*

Computational Marine Hydrodynamics Lab, School of Naval Architecture, Ocean and Civil Engineering
Shanghai Jiao Tong University, Shanghai, China

This paper numerically investigates breaking wave interaction with a vertical wall attached with a recurved parapet in 1:8 model scale, as part of the ISOPE-2022 comparative study. The in-house CFD solver naoe-FOAM-SJTU based on the open source platform OpenFOAM is used to perform all simulations. For wave generation, a novel generating-absorbing boundary condition (GABC) is adopted to replace the time-consuming moving boundary wavemaker. A geometric volume-of-fluid (VOF) method based on piecewise-linear interface calculation (PLIC) is incorporated in the present numerical model to capture the sharp interface and improve the accuracy of the predicted impact pressure. The time history and frequency analysis of the wave elevation and pressure at each probe are compared with the experimental data. The comparison demonstrates that the present numerical model is able to predict the impact pressure with sufficient accuracy but gives less accurate results of wave elevation. Moreover, the evolutions of free surface, pressure, and vorticity distribution are further provided to achieve a better understanding of this complex wave-structure interaction issue as a good complement to the experiments.

INTRODUCTION

Vertical breakwaters are typical coastal structures intended to reduce the effects of incoming waves, especially in extreme sea conditions. In practical design, wave overtopping has been a significant issue of sustained concern for decades. Among the various solutions, a parapet fixed on the top of the vertical wall has been proven effective by deflecting back the up-rushing water seawards. However, according to previous studies, the shape and parameters of the parapet will significantly influence the impact force and pressure compared with the original vertical wall. To provide guidelines to predict the wave impact and wave loading, it is necessary to systematically investigate the variations under different wave conditions, including non-breaking and broken waves.

As a representative shape, the recurved parapet has gradually attracted more attention recently. Kortenhaus et al. (2002, 2003) highlighted the effectiveness of the recurves and parapets in wave overtopping through abundant experimental data collected in the wave flume of the Leichtweiß-Institute. Nevertheless, they pointed out that their existences may increase the wave loadings on the vertical wall. Ravindar et al. (2019) conducted large-scale (1:1) experiments to characterize the impact pressure under different wave breaking conditions at the Coastal Research Centre (FZK), Germany. According to their classification, the breaker types can be divided into three conditions: slightly breaking waves (SBW), breaking waves with small air trap (BWSAT), and breaking waves with large air trap (BWLAT). In addition, they reported the significant effect of the entrained air on the impact pressure. On this basis, Ravindar and Sriram (2021) and Ravindar et al. (2021) carried out small-scale (1:8) experiments in the Department of Ocean Engineering at the Indian Institute of Technology

Madras, Chennai, Tamil Nadu, India. They analyzed the scale effects and proposed a combined Cuomo-Froude method for scaling up the impact pressure of small-scale results. Besides, they also discussed the impact pressure and forces of different types of parapets under the above-classified wave breaking conditions. Formentin et al. (2021) performed two-dimensional small-scale laboratory experiments to investigate wave overtopping at smooth berms with crown walls, focusing on wave loads and overtopping discharges. In their parametric study, the inclusion of parapets was also considered.

Considering the scale effect and the possible entrained air pocket, more and more scholars have adopted various numerical approaches to investigate the detailed behaviors of this problem. Castellino, Lara, et al. (2018) and Castellino, Sammarco, et al. (2018) used the single-phase solver IH2VOF and the two-phase solver IHFOAM to conduct a series of two-dimensional simulations of a vertical breakwater with a recurved parapet under non-breaking waves. They identified an impulsive phenomenon referred to as “confined-crest impact” and further performed a sensitivity study on the parameters of the recurved parapet. On this basis, Castellino et al. (2021) further investigated the mechanisms behind the “confined-crest impact” and extended Goda’s formulae to account for such impulsive events on recurved parapets. Liu et al. (2019) used a two-phase compressible CFD solver with the Ghost Fluid Method (GFM) and a free surface turbulence model to explore the violent breaking wave impacts on a vertical wall. In their solver, the air compressibility was taken into account, thus being more physical under wave breaking conditions. Among four considered breaking conditions, they observed that the maximum wave forces appear in the “flip-through” and “large air pocket” cases. Molines et al. (2020) numerically investigated the influence of parapets on crown walls of mound breakwaters with parapets using OpenFOAM. Consistent with the previous studies, the dimensionless horizontal forces and overturning moments increased with the presence of the parapet. For meshless methods, Altomare et al. (2015) used DualSPHysics, an SPH-based numerical model, to investigate wave loading on different types of coastal structures with a moving boundary wavemaker. The good agreement with the formulae predictions and experimental results proved its capability on such problems. Similarly,

*ISOPE Member; †Corresponding author.

Received August 10, 2022; updated and further revised manuscript received by the editors September 19, 2022. The original version (prior to the final updated and revised manuscript) was presented at the Thirty-second International Ocean and Polar Engineering Conference (ISOPE-2022), Shanghai, China (virtual), June 5–10, 2022.

KEY WORDS: Breaking waves, recurved parapet, naoe-FOAM-SJTU, generating-absorbing boundary condition (GABC), geometric VOF method.

Ma et al. (2022) also adopted DualSPHysics to study the impact of plunging breaking waves on the inverted L-shaped breakwater with the improvements by GPU and dynamic boundary particles.

In the present study, the in-house CFD solver naoe-FOAM-SJTU is used to simulate the wave-structure interaction between breaking waves and a vertical wall attached with a recurved parapet in model scale, which was part of the comparative study in the ISOPE-2022 conference. The primary objective is to validate the accuracy of naoe-FOAM-SJTU in simulating these violent free surface flows. The remainder of this paper is organized as follows. First, the numerical methods are introduced briefly, including the governing equations, interface capturing method, and wave generation approach. Then, the numerical setup is described in detail. In the following section, the results and discussion are presented in terms of the wave elevation, impact pressure, and flow field. Finally, the main conclusions are drawn.

NUMERICAL METHODS

The in-house marine hydrodynamics CFD solver naoe-FOAM-SJTU based on the open source platform OpenFOAM is used to conduct the simulation. Compared with other conventional OpenFOAM solvers like IHFOAM, naoe-FOAM-SJTU mainly aims to solve complex marine engineering problems, thus incorporating a self-developed six-degree-of-freedom (6DOF) rigid body motion module, a Suggar++-based dynamic overset grid module, and a mooring line module. In addition, we also develop and provide interfaces to a wide range of third-party libraries, including the wave2Foam, HOS-NWT, and HOS-ocean. Its accuracy and reliability have been validated in many complex practical problems, such as ship hull-rudder-propeller interaction, ship maneuverability, wave-structure interaction (WIC), vortex-induced motion (VIM), and so on (Cao and Wan, 2017; Chen et al., 2022b; Shen et al., 2015; Wang and Wan, 2018; Wang et al., 2019; Zhao et al., 2018, 2022; Zhuang et al., 2022). Recently, the solver has been upgraded to the framework of OpenFOAM v8.

Governing Equations

In the present study, the flow is described by the two-phase incompressible Navier-Stokes equations as given below.

$$\nabla \cdot \mathbf{U} = 0 \quad (1)$$

$$\frac{\partial \rho \mathbf{U}}{\partial t} + \nabla \cdot (\rho \mathbf{U} \mathbf{U}) = -\nabla p_d - \mathbf{g} \cdot \mathbf{x} \nabla \rho + \nabla \cdot (\mu \nabla \mathbf{U}) + \mathbf{f}_\sigma \quad (2)$$

where \mathbf{U} is the velocity, ρ is the weighted averaged density, \mathbf{g} is the acceleration of gravity, \mathbf{x} is the coordinate vector, and $p_d = p - \rho \mathbf{g} \cdot \mathbf{x}$ is the dynamic pressure. μ is the molecular viscosity. \mathbf{f}_σ is the surface tension term defined as

$$\mathbf{f}_\sigma = \sigma \kappa \nabla \alpha_v \quad (3)$$

where the surface tension coefficient σ is set to 0.07 N/m, $\kappa = -\nabla \cdot (\nabla \alpha_v / |\nabla \alpha_v|)$ is the interface curvature, and α_v is the phase fraction in the VOF method.

Interface Capturing Method

To accurately capture the interface, the volume-of-fluid (VOF) method (Rusche, 2003) is adopted in the present study. The transport equation is given below.

$$\frac{\partial \alpha_v}{\partial t} + \nabla \cdot (\alpha_v \mathbf{U}) = 0 \quad (4)$$

where α_v is the phase fraction of the specified phase in each cell. Taking the air-water two-phase flow as an example, $\alpha_v = 1$ and 0 represents the water and air, respectively. When $0 < \alpha_v < 1$, it represents the interface region between the water and air. In the following analysis, $\alpha_v = 0.5$ is regarded as the free surface to calculate the wave elevation at each probe.

In order to solve Eq. 4 without excessive numerical diffusion, a geometric VOF method based on piecewise-linear interface calculation (PLIC) is employed to obtain a sharp interface. (In the present study, the interface thickness, i.e., the distance between the iso-surfaces of $\alpha_v = 0.01$ and $\alpha_v = 0.99$, is about three mesh grids.) This VOF method has already been available in OpenFOAM v8 as a series of new surface interpolation schemes for the phase fraction α_v . Compared with other pure geometric methods, it can fall back to the interface-compression algebraic approach (Weller, 2008) when the interface cannot be fully resolved. This strategy can enhance robustness in dealing with practical engineering problems. For a detailed description, refer to Chen et al. (2022a).

Wave Generation

In the present numerical model, a novel generating-absorbing boundary condition (GABC) is used for wave generation. This boundary condition has been implemented by Borsboom and Jacobsen (2021) in the third-party library wave2Foam (Jacobsen et al., 2012), based on the previous work by Wellens and Borsboom (2020). Compared with the original relaxation zone technique, it does not require the additional domain to dampen the waves at the outlet, thus saving computational cost. Moreover, this boundary condition is also capable of generating a variety of waves, including regular, irregular, and solitary waves.

The basic formulas are briefly introduced below. This boundary condition is based on the classical Sommerfeld radiation condition.

$$\frac{\partial \phi}{\partial t} + c(z) \frac{\partial \phi}{\partial x} = 0 \quad (5)$$

where ϕ is the velocity potential, and $c(z)$ is a depth-varying function instead of a constant c , which is proposed for dispersive waves. When Eq. 5 is adopted into the Navier-Stokes framework, we can finally obtain a dynamic pressure condition

$$\left(1 + \frac{\rho c(z)}{\Delta} \left(\frac{1}{a_p}\right)_b\right) (p_d)_b = \frac{\rho c(z)}{\Delta} \left(\frac{1}{a_p}\right)_b (p_d)_c + c(z) \rho \frac{(\mathbf{H}(\mathbf{u}_N))_b}{(a_p)_b} - S_G \quad (6)$$

where ρ is the weighted averaged density equal to that in Eq. 2, $(\)_b$ denotes the variables on the boundary face, $(\)_c$ denotes the variables of the owner cell of the boundary face, $1/a_p$ is the diagonal coefficient of the semi-discretized form of Eq. 2, $\mathbf{H}(\mathbf{u}_N)$ consists of the source term and the contribution from all neighbor cells, and S_G is the source term for wave generation. Although wave absorption at the outlet is not required in the present working condition, its low reflection coefficient achieved in different wave propagation cases has been validated in Borsboom and Jacobsen (2021). Recently, its modified variant, coupled with the Ghost Fluid Method (GFM), has been successfully applied to the numerical simulations of the wave-structure interaction problem (Chen et al., 2022b).

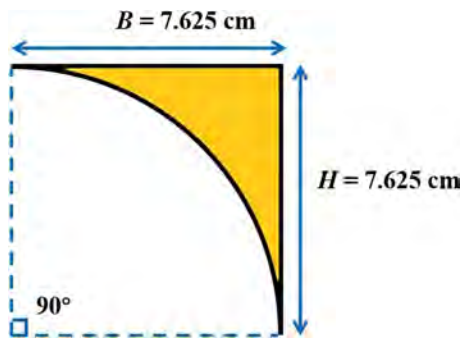


Fig. 1 Geometric model of recurved parapet

NUMERICAL SETUP

In this comparative study, the wave flume experiments were performed in the Department of Ocean Engineering at the Indian Institute of Technology Madras, Chennai, Tamil Nadu, India. The main dimensions of this wave flume are 72.5 m \times 2.0 m \times 2.5 m (length \times width \times depth). A piston-type wave-maker and a beach are used in this wave flume to generate and absorb waves, respectively. In our simulations, the numerical setup is basically consistent with the experiments, which will be described accordingly in the following subsections. More details about the experiments can be found in Ravindar et al. (2022).

Computational Domain and Mesh

Figure 1 schematically shows the geometric model of the recurved parapet. Its arch is a quarter of a circle, so the horizontal length B and vertical height H are both 7.625 cm. In the experiments, this recurved parapet was fixed on the top of a vertical wall at the end of the wave flume, as shown in Fig. 2. In the present simulation, a two-dimensional computational domain with only one cell in the lateral direction (y -axis) is adopted to save computational cost. Other parameters are basically consistent with those of the wave flume. The origin of the coordinate system is at the intersection of the structure and the free surface at still water.

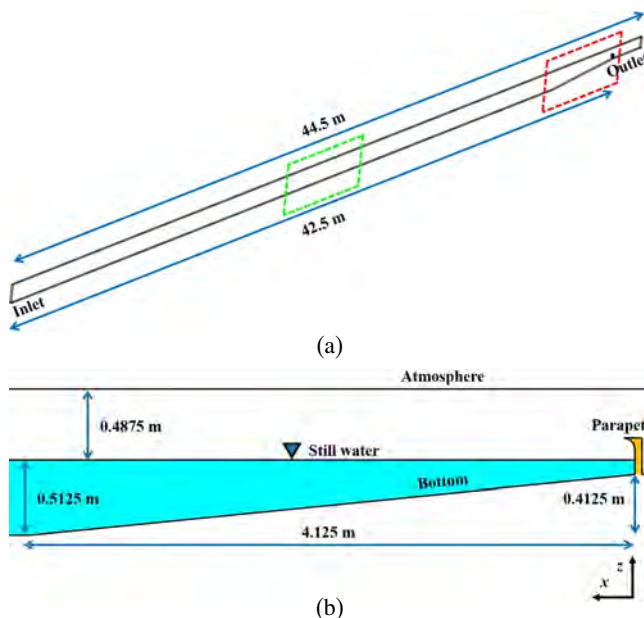


Fig. 2 Computational domain: (a) overview and (b) magnified view indicated by red dashed box

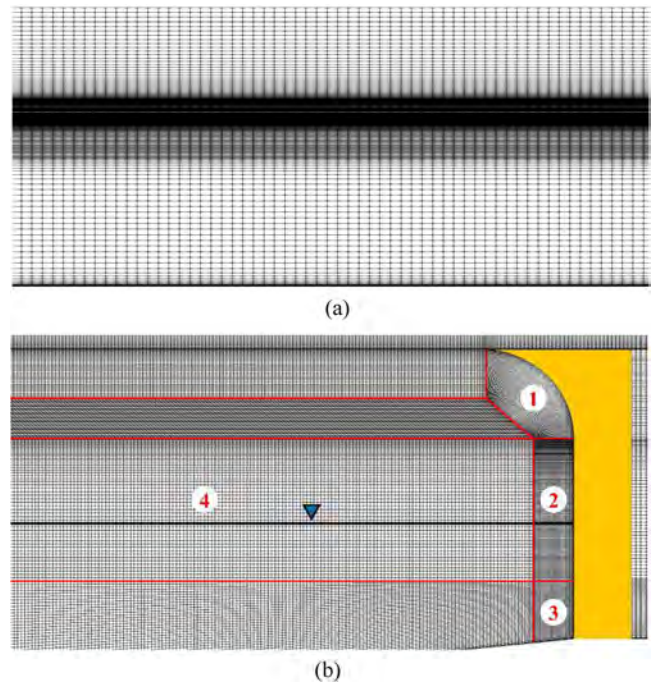


Fig. 3 Computational mesh: (a) magnified view of wave propagation region indicated by green dashed box and (b) magnified view near parapet indicated by red dashed box in Fig. 2a

In Fig. 2a, an overall view of the computational domain is presented. The distance between the inlet and the structure is 42.5 m, leaving a length of 2 m before the outlet. Figure 2b further gives a magnified view near the parapet indicated by the red dashed box. The wave propagation region has a constant working depth of 0.5125 m, followed by a 1:10 slope in front of the parapet. The top of the computational domain is 0.4875 m above the still water, approximately the working depth.

To obtain a high-fidelity flow field, a two-dimensional block-structured mesh is adopted for simulation, as shown in Fig. 3. The bold black line represents the free surface at still water, and the red lines depict the topology of blocks. The present mesh consists of 4.6×10^5 cells, in which the configuration is mainly based on wave propagation in the far field and wave breaking in the near field.

Figure 3a shows the magnified view of the wave propagation region, which is indicated by the green dashed box in Fig. 2a. The main purpose of the following mesh configuration is to minimize the numerical dissipation in wave propagation at a reasonable resolution, which is also well validated in Fig. 6. In the horizontal direction, the uniform length is approximately $1/115\lambda$, where λ is the wavenumber. In the vicinity of the free surface, the uniform mesh height is approximately $1/30 h$, where h is the wave height. To save computational cost, the mesh gradually becomes coarse when approaching the atmosphere. However, given the present intermediate depth condition, the bottom effect cannot be ignored. Therefore, the height of the first near-wall layer on the bottom is set to 5×10^{-4} m, and the corresponding expansion ratio is set to 1.3.

Figure 3b further shows the magnified view near the recurved parapet, with the main focus on capturing such small-scale wave-breaking phenomena of interest. Three blocks are used to capture the feature edges of the vertical wall and parapet, which are blocks 1, 2, and 3, respectively. The height of the first near-wall layer is set to 4×10^{-4} m, and the corresponding expansion ratio is set to 1.2. Moreover, to improve the aspect ratio, blocks 1 and 2 are

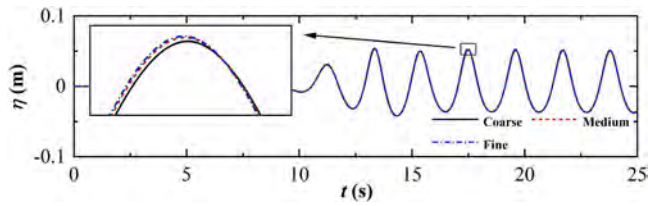


Fig. 4 Mesh convergence study at WPB6

of the higher mesh level in the vertical direction. This refinement is mainly because of the wave-breaking phenomenon that occurs in these regions. For the same reason, the cells in block 4 have a uniform size of 3×10^{-3} m.

To verify the current configuration, a mesh convergence study is performed in Fig. 4. Three different sets of meshes with a refinement ratio of approximately 1.25 are adopted: coarse (3.6×10^5 cells), medium (4.6×10^5 cells), and fine (5.6×10^5 cells). Through the comparison of wave elevation at WPB6, it can be observed that the results of the medium and fine meshes are almost the same, while the coarse mesh under-predicts the peak amplitudes. Therefore, the medium mesh is sufficient for the present working condition, which will be adopted in the following simulations.

Working and Boundary Conditions

In the present study, the input wave is a monochromatic Stokes second-order regular wave with a wave height h of 0.0875 m and a wave period T of 2.1 s. Moreover, according to the experimental setup, six wave probes are used to record the wave elevation η at different positions, as listed in Table 1. In the experiments, their sampling frequency f is 100 Hz, and in our simulations, the output interval is each time step. Among them, the time history of wave elevation at WPB6 will be first compared with the experimental measurement and theoretical solution to validate the GABC boundary condition. In addition, seven pressure probes (sampling frequency $f = 9600$ Hz), with four on the vertical wall ($x = 0$) and three on the recurved parapet ($x \neq 0$), are mounted on the structure to record the impact pressure. Table 2 lists their specific coordinates, and Fig. 5 further illustrates the relative posi-

Wave Probe	x (m)
WPB1	0.83
WPB2	4.62
WPB3	5.08
WPB4	5.66
WPB5	11.5
WPB6	24.5

Table 1 Location of wave probes

Pressure Probe	x (m)	z (m)
PP1	0	-0.075
PP2	0	-0.0325
PP3	0	0.01
PP4	0	0.0525
PP5	0.005	0.1
PP6	0.022	0.1262
PP7	0.077	0.1475

Table 2 Location of pressure probes on structure

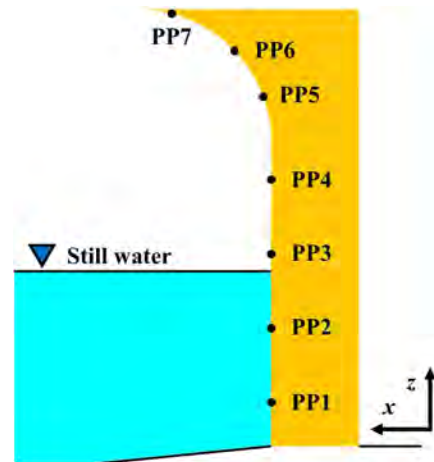


Fig. 5 Illustration of pressure probes on structure

tions on the structure. Since the duration of each impact event is very short, the pressure is also output at each time step.

For the boundary conditions, the GABC boundary condition is applied to the inlet for wave generation. The no-slip boundary condition is imposed on the structure and bottom, the Neumann boundary condition $\partial\phi/\partial n = 0$ (zeroGradient condition) is used for the atmosphere and outlet, and the empty boundary condition is adopted for the lateral sides (not shown in Fig. 2).

For the temporal discretization, a blended scheme between the first-order Euler scheme and the second-order Crank-Nicolson scheme is adopted. The blending factor is set to 0.95 to avoid excessive numerical dissipation during wave propagation (Zhuang and Wan, 2021). For the spatial discretization, the second-order linear scheme is employed for the advection and diffusion terms in the momentum equation. Note that a PLIC corrected scheme is applied to the phase fraction transport equation. According to previous numerical studies under similar conditions (Castellino, Sammarco, et al., 2018; Liu et al., 2019), the maximum Courant–Friedrichs–Lewy number is usually in the range of 0.3–0.5. Therefore, an adjustable time step is used in this study to maintain a balance between accuracy and stability, which ensures the maximum Courant–Friedrichs–Lewy number is below 0.2 ($\Delta t \sim 10^{-5}$ s). The total simulation time t is 50 s, which gives sufficient periodic results for statistical analysis.

RESULTS AND DISCUSSION

Wave Elevation

To validate the incident wave generation, Fig. 6 first shows the wave elevation at WPB6 when the reflected waves have not arrived. Here, the experimental measurement and theoretical solution are both given. Note that the measured time series have been aligned in time for a better comparison. In general, the numerical result achieves a good agreement, demonstrating the good

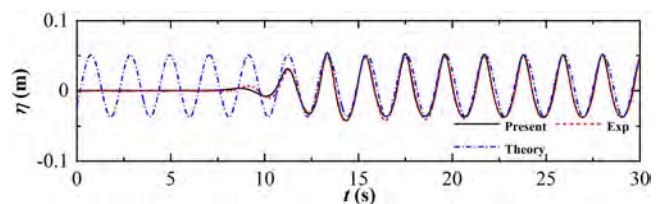


Fig. 6 Comparison of wave elevation at WPB6

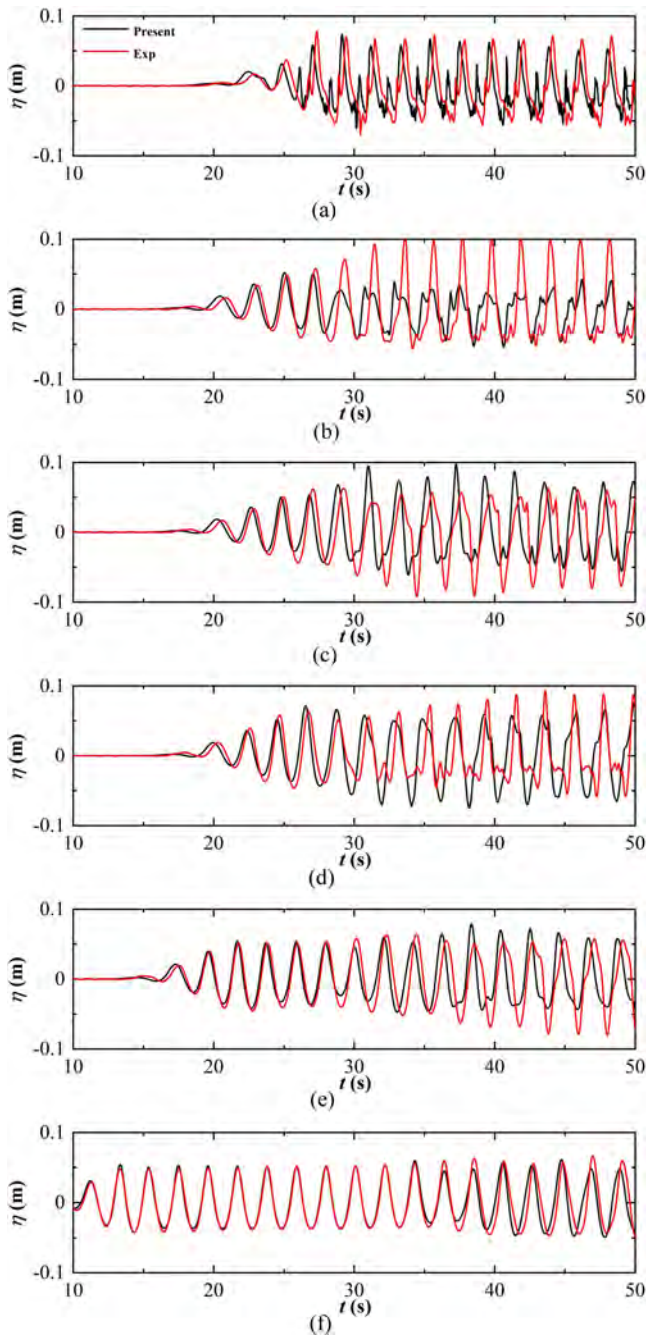


Fig. 7 Time histories of wave elevation at (a) WPB1, (b) WPB2, (c) WPB3, (d) WPB4, (e) WPB5, and (f) WPB6

performance of the GABC boundary condition. The slight phase discrepancy with the wave theory is possibly due to the cumulative numerical dissipation over a long distance and the reported spurious air velocities (Afshar, 2010).

Figure 7 shows the time series of wave elevation at each probe to investigate the reflected wave characteristics. As shown in Fig. 7a, the complex shape due to nearby wave breaking, i.e., primary and secondary peaks within one wave cycle, is well captured by the present numerical model. For the location far from the structure, i.e., WPB6, Fig. 7f shows that the predicted wave elevation also agrees well with the experimental data. However, for the rest of the wave probes, significant discrepancies can be observed when the reflected waves interact strongly with the incident ones. Although the phases are roughly the same, the amplitudes still indicate that the present model cannot fully capture the

reflected wave characteristics. We think there are two main reasons: three-dimensional and turbulence effects.

Considering such a long computational domain and the corresponding small time step for stability, we have to adopt the two-dimensional simulations in the present study. However, due to the large width (2.0 m) of the wave flume in the experiment, the two-dimensional assumption cannot hold in the region where reflected waves dominate, such as WPB2-WPB4. In other words, the reflected waves are likely to show strong three-dimensionality. In this regard, Zheng and Zhao (2022) also simulated this problem using their three-dimensional parallel CIP-based numerical model with the large eddy simulation method. Their visualization of free surface shape demonstrated that the wave breaks and spreads with strong three-dimensional characteristics. Furthermore, this three-dimensional effect can also be observed in similar working conditions. In a previous experimental investigation of wave impact on vertical walls with parapets (Frandsen et al., 2016), their recorded video (<https://www.youtube.com/watch?v=ue7qSURsBs4>; uploaded April 6, 2017) clearly showed that when the first incident wave hit the structure, the free surface profile quickly become three-dimensional due to the violent breaking waves and their subsequent interactions with the following incident waves.

On the other hand, it is believed that the turbulence effect plays an important role in the cases of wave breaking. Liu et al. (2020) found that the turbulence models have large influences on the breaking position and wave elevations, which can make a better match with the experiments. In this regard, Li et al. (2022) used the SST $k-\omega$ model to simulate the same problem, achieving better agreement in terms of wave elevation. However, the

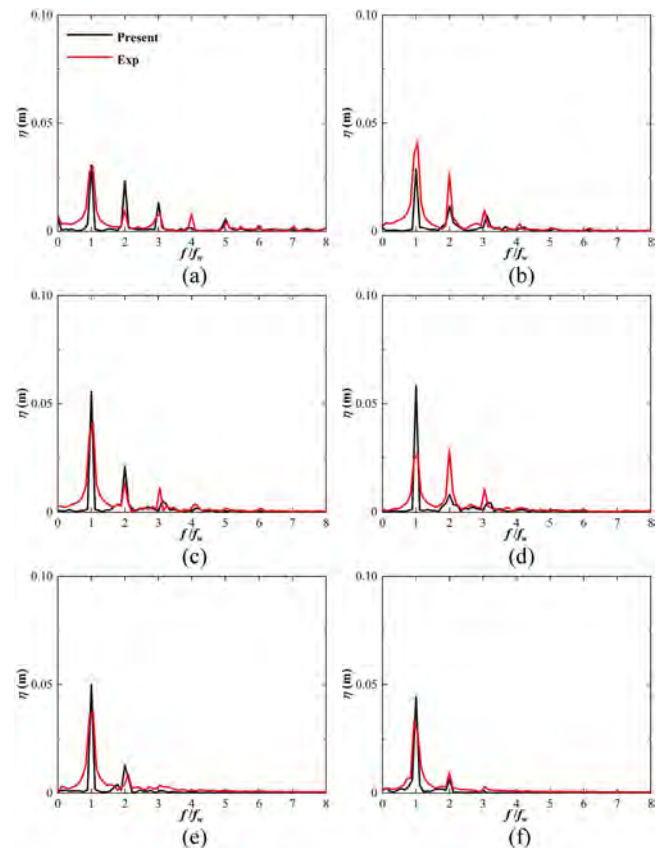


Fig. 8 Spectral analysis of wave elevation at (a) WPB1, (b) WPB2, (c) WPB3, (d) WPB4, (e) WPB5, and (f) WPB6

impact pressure was reported to be under-predicted in their simulations. This is mainly because the original RANS models also cause severe numerical damping due to the over-estimated turbulence viscosity μ_t (Devolder et al., 2017; Larsen and Fuhrman, 2018). Nevertheless, due to the constraint of the two-dimensional assumption, the LES or DES approaches are not strictly applicable in our simulations. Thus, to accurately capture the reflected wave characteristics, it is necessary to perform three-dimensional simulations using the LES or DES methods.

Figure 8 further gives the spectral analysis results using the Fast Fourier Transform (FFT) method. Note that the results are all non-dimensionalized by the incident wave frequency f_w for better visibility. While the discrepancies in the time domain do exist, the present numerical model can reasonably predict the reflected wave characteristics in the frequency domain. When the probes are far from the structure, i.e., WPB5 and WPB6, Figs. 8e and 8f show that the dominant frequencies are still the significant first harmonic (f_w), suggesting the wave elevations are less affected by the reflected components. When gradually approaching the structure, the third harmonic appears and grows due to the interaction between the incident and reflected waves, as shown in Figs. 8c and 8d. This nonlinear phenomenon also manifests as small secondary peaks at the crests and troughs in the time series, as previously shown in Figs. 7c and 7d. When closest to the structure, i.e., at WPB1, the high-order harmonics increase rapidly, and higher components are newly identified in the spectrum (see Fig. 8a), including the 5th and 6th ones. This trend is due to the violent free surface deformation caused by the nearby wave breaking, which will also be visualized later. In addition, it is worth mentioning that some phase shifts can be observed for harmonics, especially for the high-order components. We believe that this is mainly due to the significant difference in sampling frequency between experiments (10^2 Hz) and numerical simulations ($\sim 10^5$ Hz).

Impact Pressure

To investigate the wave impact, the time-histories of pressure at each probe are given in Fig. 9. The left column is the overall views, and the right column is the magnified views during one impact event. It is clear from the comparison that the predicted impact pressure agrees well with the experiment in general. For all probes, the peak value of each event is statistically of the same order of magnitude as the measurement, and the main characteristics of the time histories are also basically captured. Given these facts, it can be concluded that the present numerical model is sufficient to predict the impact pressure within reasonable accuracy. That is, the non-negligible three-dimensional and turbulence effects mentioned above have little influence on the wave impact.

After validating the capability of our numerical model, we focus on the specific characteristics of different representative positions. According to previous studies, a typical time history of pressure during one impact can be characterized as three parts in sequence: impact pressure, oscillatory pressure, and quasi-static pressure. Because PP1–4 are below or near the free surface at still water, the water tongues of plunging breakers hit these positions directly. As a result, the impact peak pressure reaches very high within a short duration, as shown in Figs. 9a–9d. At the same time, the quasi-static stage is relatively long due to the sustained contact with the water. Moreover, in the present wave condition, the entrapped large air pocket (see Fig. 11) is responsible for the negative sub-atmospheric pressure, as indicated by the black arrow in Fig. 9c. On the other hand, for the probes on the recurved parapet, i.e., PP5–7, the peak pressure is reduced, and the quasi-static stage becomes short due to the high-speed jet.

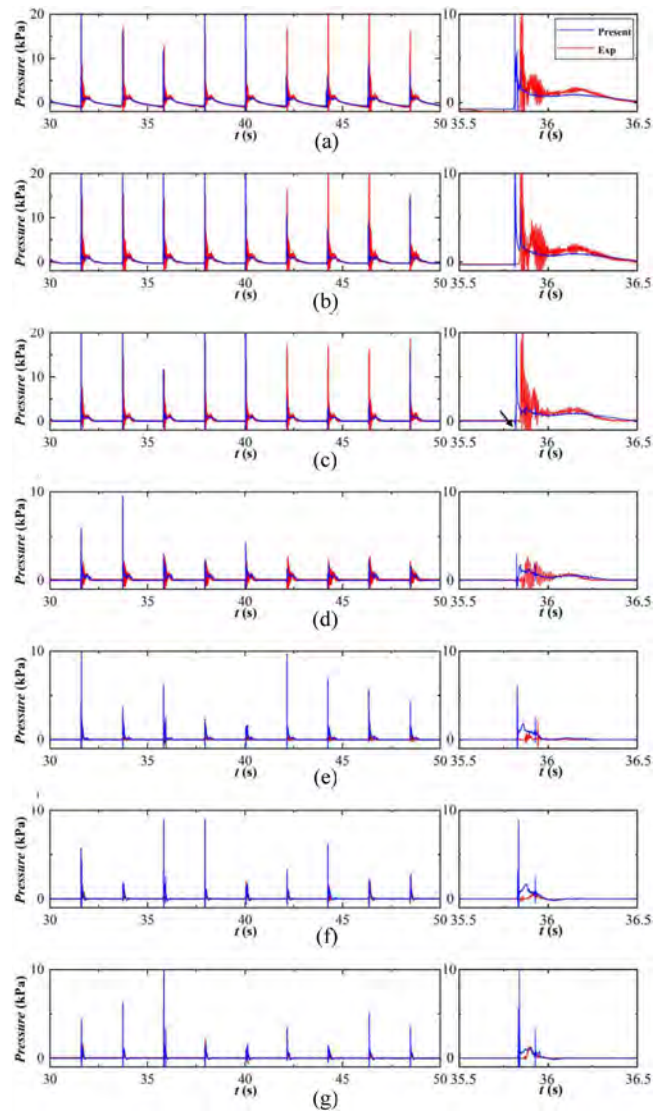


Fig. 9 Time histories of pressure at (a) PP1, (b) PP2, (c) PP3, (d) PP4, (e) PP5, (f) PP6, and (g) PP7

However, it should be noted that the expected oscillatory pressure caused by the expansion and compression of the air pocket is not as obvious as in the experiment. This discrepancy is because the present numerical model is based on the assumption of incompressibility and thus can only roughly capture the overall trend of the averaged value. To our knowledge, when air compressibility is further taken into account in the numerical model (Liu et al., 2019), this problem can be much improved. However, Liu et al. (2019) pointed out that even when considering air compressibility, the presence of air escape and dispersed air bubbles in the experiments would greatly affect the prediction of impact pressure. Therefore, it poses challenges to the interface capturing method, which should be improved in future high-fidelity numerical simulations. Furthermore, it is worth noting that the scale effect may also play an important role in air compressibility, which is also one of the main concerns in this ISOPE-2022 comparative test.

Flow Field Evolution

To further explore the mechanism, the flow field evolution during one wave impact is visualized in this section. Before the analysis, the instantaneous free surface profile is first compared with

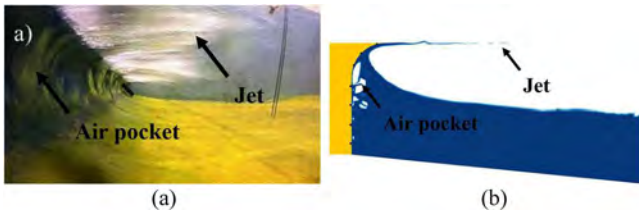


Fig. 10 Comparison of free surface profile: (a) experimental photo and (b) numerical result at $t = 35.86$ s

the experiments in Fig. 10. At this time instant, the horizontal jet and entrained air pocket can be clearly observed in the experimental photo. In this regard, the present numerical model captures these two significant features well.

Figure 11 shows the instantaneous free surface for a sequence of time instants, colored by the velocity magnitude $|\mathbf{U}|$. (For clarity, Fig. 11 only retains the quantities in the water phase.) Correspondingly, Fig. 13 and Fig. 12 show the contours of vorticity and pressure, respectively. Here, the black points on the structure denote the above-listed pressure probes. Before reaching the structure, a plunging breaker with high velocity magnitude has already been formed, as shown in Fig. 11a. When the tongue of the plunging breaker subsequently hits the vertical wall, Fig. 11b shows that it entraps a lot of air and encloses up to form a large air pocket. With this important feature, the present breaking condition belongs to a classified one proposed by Ravindar et al. (2019), i.e., breaking wave with a large air trap (BWLAT). Meanwhile, this impact by the wave tongues creates the high-pressure regions colored dark pink, as shown in Fig. 12b, which corresponds to the peak pressure in Fig. 9. After that, some water with high kinetic energy (red regions in Fig. 11c) rises upwards rapidly along the vertical wall and hits the recurved parapet. Then, Fig. 11d shows that the up-rushing water is deflected back towards the incident direction by the parapet, resulting in a thin horizontal high-speed jet. At the same time, the entrapped large air pocket disperses into several small pockets and bubbles after expansion and compression. They are transported upwards with the water and collapse on

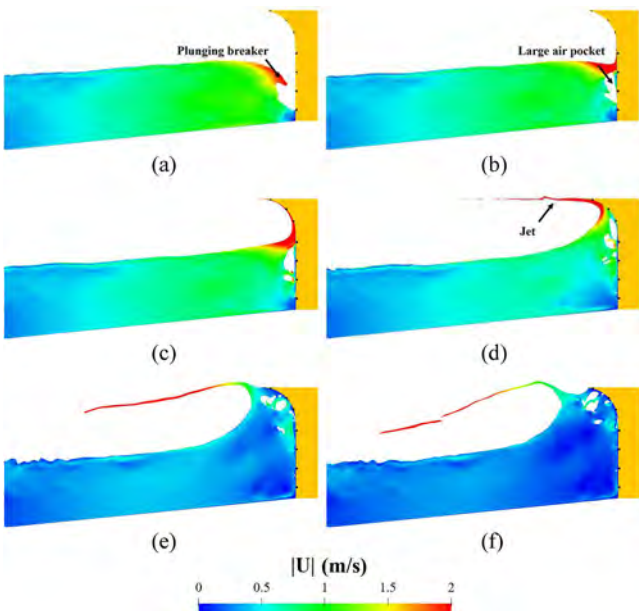


Fig. 11 Instantaneous velocity magnitude during one wave impact at (a) $t = 35.78$ s, (b) $t = 35.8$ s, (c) $t = 35.82$ s, (d) $t = 35.86$ s, (e) $t = 35.96$ s, and (f) $t = 36.02$ s

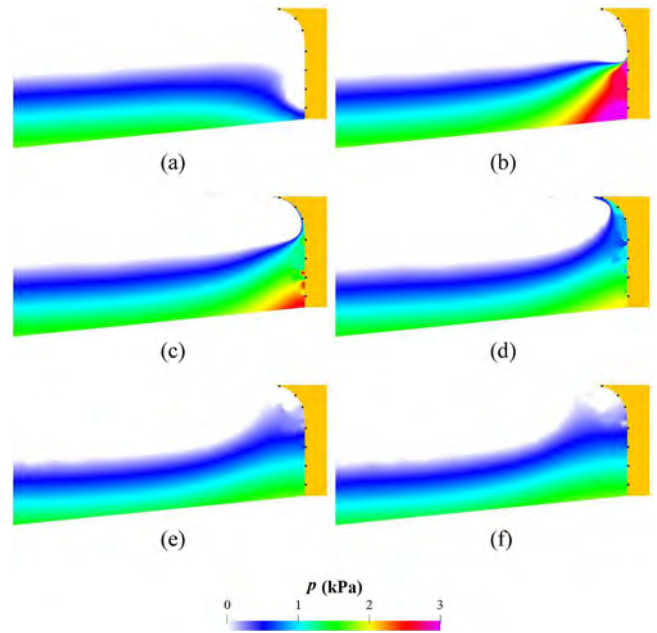


Fig. 12 Contours of pressure during one wave impact at (a) $t = 35.78$ s, (b) $t = 35.8$ s, (c) $t = 35.82$ s, (d) $t = 35.86$ s, (e) $t = 35.96$ s, and (f) $t = 36.02$ s

the recurved parapet. These physical phenomena can well explain the negative sub-atmospheric pressure and the subsequent small oscillations in Fig. 9. In Fig. 12, they result in a chaotic distribution around the structure. Similar to the current case, Kiger and Duncan (2012) have systemically summarized the air-entrainment mechanisms behind the plunging breaking waves in the absence of structure, which can help us to better understand the present problem. Moreover, along with air entrainment, the vortices induced by breaking waves are also of great research interest, as shown in Fig. 13. It can be observed that the vorticity magnitude is strong where the air pockets and bubbles are located. This strong cor-

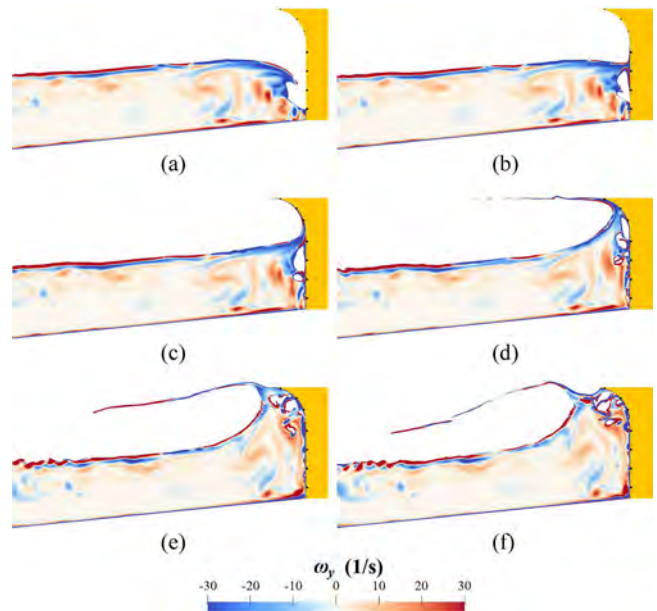


Fig. 13 Instantaneous vorticity during one wave impact at (a) $t = 35.78$ s, (b) $t = 35.8$ s, (c) $t = 35.82$ s, (d) $t = 35.86$ s, (e) $t = 35.96$ s, and (f) $t = 36.02$ s

relation has also been demonstrated in previous numerical investigations (Lubin et al., 2006; Watanabe et al., 2005). It is also worth mentioning that Lubin et al. (2006) pointed out that three-dimensional simulations have different behaviors in terms of vortices and turbulence dissipation, which also highlights the need for three-dimensional simulations in the future.

CONCLUSIONS

In this paper, the wave-structure interaction between breaking waves and a vertical wall attached with a recurved parapet is simulated by our in-house CFD solver naoe-FOAM-SJTU. For wave generation, a generating-absorbing boundary condition (GABC) is used to save computational cost. To capture a sharp interface, a PLIC-based geometric VOF method is adopted. The incorporation of these two methods can improve the accuracy and computational efficiency of wave-structure interaction (WSI) simulations.

At WPB6, the numerical results are first compared with the theoretical solution of the wave theory and experimental data to validate the wave generation. Then, the numerical results of wave elevation and pressure in the time and frequency domains at the prescribed probes are compared with the experiment to assess the capability of the present numerical model. On this basis, the contours of the flow field evolution are shown to gain insight into the reflection characteristics and wave impact. The main conclusions are as follows.

The comparison with the experimental measurements indicates that the present numerical model can predict the impact pressure in terms of the overall trend and the order of peak magnitude but cannot fully resolve the reflected waves in the time domain (but achieves reasonable agreement in the frequency domain). This problem can be mainly attributed to the non-negligible three-dimensional effect for the reflected waves and the potential turbulence effect with the presence of wave breaking. These findings from our preliminary work can help to improve the established numerical model in the near future.

For the detailed flow characteristics, when the locations are far from the structure, the wave elevation is still dominated by the incident component. However, when approaching the structure, the nonlinearity of wave elevation increases rapidly, which manifests as significant high-order harmonics in the frequency spectrum. This phenomenon is particularly evident at WPB1. For the impact pressure on the structure, a large-amplitude and short-duration peak can be observed below or near the free surface at still water. On the other hand, the wave impact on the recurved parapet can be characterized as reduced peak pressure and a short quasi-static stage. Visualization of the flow field further shows that after the tongue of the plunging breaker with high velocity magnitude hits the structure, a large air pocket is entrapped, which then undergoes expansion and compression. Meanwhile, a thin horizontal high-speed jet is created when the uprushing water is deflected back by the recurved parapet. These phenomena can well explain the characteristics in the time-histories of pressure, including large-amplitude peaks, negative sub-atmospheric pressure, and oscillations. Moreover, the vorticity distribution shows its strong correlation with air pockets and bubbles. In the future, apart from the under-resolved problems mentioned above, we will also focus on improving our numerical model with corresponding high-fidelity methods, such as the capability of air compressibility and the implementation of the Ghost Fluid Method.

ACKNOWLEDGEMENTS

This work was supported by the National Natural Science Foundation of China (51909160, 51879159, 52131102) and the

National Key Research and Development Program of China (2019YFB1704200), to which the authors are most grateful.

REFERENCES

- Afshar, MA (2010). *Numerical Wave Generation in OpenFOAM®*, MS Thesis, Chalmers University of Technology, Gothenburg, Sweden.
- Altomare, C, et al. (2015). “Applicability of Smoothed Particle Hydrodynamics for Estimation of Sea Wave Impact on Coastal Structures,” *Coastal Eng*, 96, 1–12. <https://doi.org/10.1016/j.coastaleng.2014.11.001>.
- Borsboom, M, and Jacobsen, NG (2021). “A Generating-absorbing Boundary Condition for Dispersive Waves,” *Int J Numer Methods Fluids*, 93, 2443–2467. <https://doi.org/10.1002/fld.4982>.
- Cao, H, and Wan, D (2017). “Benchmark Computations of Wave Runup on Single Cylinder and Four Cylinders by naoe-FOAM-SJTU Solver,” *Appl Ocean Res*, 65, 327–337. <https://doi.org/10.1016/j.apor.2016.10.011>.
- Castellino, M, Lara, JL, Romano, A, Losada, IJ, and De Girolamo, P (2018). “Wave Loading for Recurved Parapet Walls in Non-breaking Wave Conditions: Analysis of the Induced Impulsive Forces,” *Coastal Eng Proc*, 1(36), 34–42. <https://doi.org/10.9753/icce.v36.papers.34>.
- Castellino, M, Romano, A, Lara, JL, Losada, IJ, and De Girolamo, P (2021). “Confined-crest Impact: Forces Dimensional Analysis and Extension of the Goda’s Formulae to Recurved Parapets,” *Coastal Eng*, 163, 103814. <https://doi.org/10.1016/j.coastaleng.2020.103814>.
- Castellino, M, Sammarco, P, et al. (2018). “Large Impulsive Forces on Recurved Parapets Under Non-breaking Waves. A Numerical Study,” *Coastal Eng*, 136, 1–15. <https://doi.org/10.1016/j.coastaleng.2018.01.012>.
- CFD Direct (2020). *Interface Capturing in OpenFOAM*, <https://cfd.direct/openfoam/free-software/multiphase-interface-capturing/>. Accessed on January 18, 2022.
- Chen, S, Zhao, W, and Wan, D (2022a). “Turbulent Structures and Characteristics of Flows Past a Vertical Surface-piercing Finite Circular Cylinder,” *Phys Fluids*, 34(1), 015115. <https://doi.org/10.1063/5.0078526>.
- Chen, S, Zhao, W, and Wan, D (2022b). “On the Scattering of Focused Wave by a Finite Surface-piercing Circular Cylinder: A Numerical Investigation,” *Phys Fluids*, 34(3), 035132. <https://doi.org/10.1063/5.0086826>.
- Devolder, B, Rauwoens, P, and Troch, P (2017). “Application of a Buoyancy-modified $k-\omega$ SST Turbulence Model to Simulate Wave Run-up Around a Monopile Subjected to Regular Waves Using OpenFOAM®,” *Coastal Eng*, 125, 81–94. <https://doi.org/10.1016/j.coastaleng.2017.04.004>.
- Formentin, SM, Palma, G, and Zanuttigh, B (2021). “Integrated Assessment of the Hydraulic and Structural Performance of Crown Walls on Top of Smooth Berms,” *Coastal Eng*, 168, 103951. <https://doi.org/10.1016/j.coastaleng.2021.103951>.
- Frandsen, J, Tremblay, OG, and Xhardé, R (2016). “Preliminary Investigations of Wave Impact on Vertical Walls with/without Parapets and Toe Protection on Deformable Beach,” *Proc 6th Int Conf Appl Phys Modell Coastal Port Eng Sci (Coastlab16)*, Ottawa, Canada, IAHR.
- Jacobsen, NG, Fuhrman, DR, and Fredsøe, J (2012). “A Wave Generation Toolbox for the Open-source CFD Library: OpenFoam®,” *Int J Numer Methods Fluids*, 70(9), 1073–1088. <https://doi.org/10.1002/fld.2726>.

- Kiger, KT, and Duncan, JH (2012). "Air-entrainment Mechanisms in Plunging Jets and Breaking Waves," *Annu Rev Fluid Mech*, 44, 563–596.
<https://doi.org/10.1146/annurev-fluid-122109-160724>.
- Kortenhaus, A, Haupt, R, and Oumeraci, H (2002). "Design Aspects of Vertical Walls with Steep Foreland Slopes," In *Breakwaters, Coastal Structures and Coastlines: Proc 7th Int Conf*, London, UK, ICE, 221–231.
- Kortenhaus, A, Pearson, J, Bruce, T, Allsop, NWH, and Van der Meer, JW (2003). "Influence of Parapets and Recurves on Wave Overtopping and Wave Loading of Complex Vertical Walls," *Proc Coastal Struct*, Portland, OR, USA, ASCE, 369–381.
[https://doi.org/10.1061/40733\(147\)31](https://doi.org/10.1061/40733(147)31).
- Larsen, BE, and Fuhrman, DR (2018). "On the Over-production of Turbulence Beneath Surface Waves in Reynolds-averaged Navier–Stokes Models," *J Fluid Mech*, 853, 419–460.
<https://doi.org/10.1017/jfm.2018.577>.
- Li, Q, Yan, S, Ma, Q, and Zhang, N (2022). "Numerical Investigation of Breaking Wave Interaction with Vertical Wall Attached with Recurved Parapet Using qaleFOAM," *Proc 32nd Int Ocean Polar Eng Conf*, Shanghai, China, ISOPE, 3, 2012–2019.
- Liu, S, Gatin, I, Obhrai, C, Ong, MC, and Jasak, H (2019). "CFD Simulations of Violent Breaking Wave Impacts on a Vertical Wall Using a Two-phase Compressible Solver," *Coastal Eng*, 154, 103564. <https://doi.org/10.1016/j.coastaleng.2019.103564>.
- Liu, S, Ong, MC, Obhrai, C, Gatin, I, and Vukčević, V (2020). "Influences of Free Surface Jump Conditions and Different $k-\omega$ SST Turbulence Models on Breaking Wave Modelling," *Ocean Eng*, 217, 107746.
<https://doi.org/10.1016/j.oceaneng.2020.107746>.
- Lubin, P, Vincent, S, Abadie, S, and Caltagirone, JP (2006). "Three-Dimensional Large Eddy Simulation of Air Entrainment under Plunging Breaking Waves," *Coastal Eng*, 53(8), 631–655.
<https://doi.org/10.1016/j.coastaleng.2006.01.001>.
- Ma, Z, Yang, Y, Zhai, G, Bao, J, and Teh, HM (2022). "A Study of the Impact of Plunging Waves on the Inverted L-shaped Breakwater Structure Based on SPH Method," *Ships Offshore Struct*, 17(3), 518–530.
<https://doi.org/10.1080/17445302.2020.1835055>.
- Molines, J, Bayón, A, Gómez-Martín, ME, and Medina, JR (2020). "Numerical Study of Wave Forces on Crown Walls of Mound Breakwaters with Parapets," *J Mar Sci Eng*, 8(4), 276.
<https://doi.org/10.3390/jmse8040276>.
- Ravindar, R, and Sriram, V (2021). "Impact Pressure and Forces on a Vertical Wall with Different Types of Parapet," *J Waterw Port Coastal Ocean Eng*, 147(3), 04021007.
[https://doi.org/10.1061/\(asce\)ww.1943-5460.0000635](https://doi.org/10.1061/(asce)ww.1943-5460.0000635).
- Ravindar, R, Sriram, V, Schimmels, S, and Stagonas, D (2019). "Characterization of Breaking Wave Impact on Vertical Wall with Recurve," *ISH J Hydraul Eng*, 25(2), 153–161.
<https://doi.org/10.1080/09715010.2017.1391132>.
- Ravindar, R, Sriram, V, Schimmels, S, and Stagonas, D (2021). "Approaches in Scaling Small-Scale Experiments on the Breaking Wave Interactions with a Vertical Wall Attached with Recurved Parapets," *J Waterw Port Coastal Ocean Eng*, 147(6), 04021034.
[https://doi.org/10.1061/\(asce\)ww.1943-5460.0000674](https://doi.org/10.1061/(asce)ww.1943-5460.0000674).
- Ravindar, R, Sriram, V, Schimmels, S, and Stagonas, D (2022). "Laboratory Study on Breaking Wave Impact on a Vertical Wall with Recurved Parapets in Small and Large Scale," *Proc 32nd Int Ocean Polar Eng Conf*, Shanghai, China, ISOPE, 3, 1991–1998.
- Rusche, H (2003). *Computational Fluid Dynamics of Dispersed Two-phase Flows at High Phase Fractions*, PhD Thesis, Imperial College London (University of London), London, UK.
- Shen, Z, Wan, D, and Carrica, PM (2015). "Dynamic Overset Grids in OpenFOAM with Application to KCS Self-propulsion and Maneuvering," *Ocean Eng*, 108, 287–306.
<https://doi.org/10.1016/j.oceaneng.2015.07.035>.
- Wang, J, and Wan, D (2018). "CFD Investigations of Ship Maneuvering in Waves Using naoe-FOAM-SJTU Solver," *J Mar Sci Appl*, 17(3), 443–458.
<https://doi.org/10.1007/s11804-018-0042-4>.
- Wang, J, Zhao, W, and Wan, D (2019). "Development of naoe-FOAM-SJTU Solver Based on OpenFOAM for Marine Hydrodynamics," *J Hydrodyn*, 31(1), 1–20.
<https://doi.org/10.1007/s42241-019-0020-6>.
- Watanabe, Y, Saeki, H, and Hosking, RJ (2005). "Three-dimensional Vortex Structures under Breaking Waves," *J Fluid Mech*, 545, 291–328. <https://doi.org/10.1017/s0022112005006774>.
- Wellens, P, and Borsboom, M (2020). "A Generating and Absorbing Boundary Condition for Dispersive Waves in Detailed Simulations of Free-surface Flow Interaction with Marine Structures," *Comput Fluids*, 200, 104387.
<https://doi.org/10.1016/j.compfluid.2019.104387>.
- Weller, HG (2008). *A New Approach to VOF-based Interface Capturing Methods for Incompressible and Compressible Flow*, OpenCFD Ltd, Report TR/HGW, 4, 35.
- Zhao, W, Wei, Z, and Wan, D (2022). "Numerical Investigation on the Effects of Current Headings on Vortex Induced Motions of a Semi-submersible," *J Hydrodyn*, 34(3), 382–394.
<https://doi.org/10.1007/s42241-022-0034-3>.
- Zhao, W, Zou, L, Wan, D, and Hu, Z (2018). "Numerical Investigation of Vortex-induced Motions of a Paired-column Semi-submersible in Currents," *Ocean Eng*, 164, 272–283.
<https://doi.org/10.1016/j.oceaneng.2018.06.023>.
- Zheng, K, and Zhao, X (2022). "Breaking Waves Interactions with Vertical Seawall Attached with Recurved Parapet Using the Three-dimensional Parallel CIP-based Model," *Proc 32nd Int Ocean Polar Eng Conf*, Shanghai, China, ISOPE, 3, 1999–2003.
- Zhuang, Y, and Wan, D (2021). "Parametric Study of a New HOS-CFD Coupling Method," *J Hydrodyn*, 33(1), 43–54.
<https://doi.org/10.1007/s42241-021-0012-1>.
- Zhuang, Y, Wang, G, Wan, D, and Wu, J (2022). "Numerical Simulations of FPSO with Sloshing Tanks in a Random Freak Waves," *J Hydrodyn*, 34(3), 491–498.
<https://doi.org/10.1007/s42241-022-0036-1>.